Theory of surface phonons at metal surfaces: recent advances

2010 J. Phys.: Condens. Matter 22 084020

(http://iopscience.iop.org/0953-8984/22/8/084020)

J. Phys.: Condens. Matter **22** (2010) 084020 (17pp) doi:10.1088/0953-8984/22/8/084020

Theory of surface phonons at metal surfaces: recent advances

G Benedek[1,2,3], M Bernasconi[1], V Chis[4], E Chulkov[2,5], P M Echenique[2,5], B Hellsing[4] and J Peter Toennies[3]

[1] Dipartimento di Scienza dei Materiali, Università di Milano-Bicocca, I-20125 Milano, Italy
[2] Donostia International Physics Center (DIPC), E-20018 Donostia/San Sebastian, Spain
[3] Max-Planck-Institut für Dynamik und Selbstorganization, D-37073 Göttingen, Germany
[4] Department of Physics, Göteborg University, Fysikgården 6B, S-412 96 Göteborg, Sweden
[5] Departamento de Fìsica de Materiales and Centro Mixto CSIC-UPV/EHU, Universidad del Paìs Vasco/Euskal Herriko Unibertsitatea, E-20018 San Sebastiàn/Donostia, Spain

Received 9 June 2009, in final form 27 July 2009
Published 5 February 2010
Online at stacks.iop.org/JPhysCM/22/084020

Abstract
Recent studies of the surface dynamics of Al(001) and Cu(111) based on density functional perturbation theory have substantiated the existence of subsurface optical phonon resonances of all three polarizations, thus confirming early predictions of the embedded-atom method. The hybridization of the shear-vertical optical resonance with the longitudinal acoustic phonon branch accounts for the ubiquitous anomalous acoustic resonance as an intrinsic feature of metal surfaces. The DFPT calculation of the phonon-induced surface charge density oscillations shows that helium atom scattering spectroscopy (HAS) can indeed probe subsurface resonances. This opens new perspectives to HAS for the measurement of subsurface phonon dispersion curves in thin films, as proved by recent HAS studies on Pb and Fe ultrathin films on copper. After discussing these recent advances, this paper briefly reviews other important trends of surface dynamics expressed in recent years.

(Some figures in this article are in colour only in the electronic version)

1. Introduction

The theory of surface phonons at metal surfaces dates back to the early measurements of surface phonon dispersion curves by means of inelastic helium atom scattering (HAS) [1–5] and electron energy loss spectroscopy (EELS) [6–10]. The early discovery by HAS of an acoustic longitudinal phonon resonance at the surface of noble metals [1, 2, 4, 5], and subsequently found with both HAS and EELS in practically all metal surfaces [5], led to the conviction that surface metal dynamics appeal to something fundamental involving surface electronic states. Simple force constant models which provide a good fit of bulk phonon dispersion curves were found to be unable to simultaneously reproduce the longitudinal resonance branch and the related HAS spectral response, unless large, unphysical perturbations of the surface force constants were considered [11–13]. This ubiquitous acoustic resonance invariably occurs well below the edge of the longitudinally polarized bulk band, even for the densely packed (111) surface of fcc metals, where no surface longitudinal mode is expected for an ideal surface with simple nearest-neighbor force constants [14]. For this reason this new surface mode was frequently referred to as anomalous longitudinal resonance (ALR).

There was another crucial aspect of the ALR which made the scenario somewhat more complicated. Whereas HAS and EELS spectroscopies agree with each other as regards the energy of the L resonance, there is, however, a substantial difference between their respective scattering amplitudes. The HAS intensity for the L resonance is quite often much larger than that for the Rayleigh wave (RW), at least up to two-thirds of the surface Brillouin zone (BZ) [3–5], whereas the EELS amplitude for the L mode is normally much smaller [7, 8]. This was regarded as a paradox (the Bortolani–Mills (BM) paradox [15]) since electrons in the inelastic impact regime are essentially scattered by the oscillation of the atom cores of the first two or three surface layers, whereas He atoms are scattered by the oscillations of the surface electron density about 2–3 Å away from the first atomic layer and should be rather insensitive to the atomic displacements parallel to the surface. In any case the ubiquitous ALR was added to the list of many important properties of metal surfaces, such

as the inward relaxation of the surface atomic layer and the surface-dependent work function, which are determined by the redistribution of the surface electronic charge with respect to the charge density in the bulk [16, 17].

As expected the above observations have stimulated extensive theoretical activity in the field of surface metal dynamics, first on the basis of semi-empirical approaches modeling in some way the coupling between the nuclear and conduction electron degrees of freedom, then by means of *ab initio* methods. Among the various semi-empirical approaches which have been largely used for two decades [5], many useful results have been obtained with the embedded-atom (EA) method [18–23] and the multipole expansion (ME) method [24–26]. The latter was particularly successful in reproducing both the surface dispersion curves and the HAS amplitudes with physically acceptable surface perturbation, while providing a convincing explanation of the BM paradox. On the other hand, the EA method, though unsuitable to provide the HAS amplitudes, was the first to correctly establish the exact nature of the ALR branch [19, 20].

The *ab initio* studies of the surface phonon dispersion curves in metals based on the density-response pseudopotential perturbation (DR-PPP) method [27–31], the frozen-phonon (FP) method [27–36] and the density functional perturbation theory (DFPT) [37] have proceeded in parallel with the development of the semi-empirical theories. A thorough discussion of these studies, with a comparison to former semi-empirical approaches, can be found in the excellent review by Heid and Bohnen [36]. Despite the intrinsic computational difficulties, *ab initio* calculations have started providing since the early 1990s a more and more satisfactory account of the experimental dispersion curves for all kinds of simple and transition metal surfaces. However the explanation of the ALR and its HAS amplitude has remained elusive, to the extent that Heid and Bohnen conjectured in their review that the acoustic resonance may arise from some special property of the He–surface interaction and not necessarily be a real spectral feature of metal surface dynamics [36].

Such a situation concerning a possible universal property of metal surfaces motivated new DFPT investigations of the phonon dispersion curves of Al(001) [38] and Cu(111) [39] surfaces, which eventually led to a conclusive elucidation of the anomalous resonance as an intrinsic feature of metal surface dynamics. These studies also recognized the ALR as playing an important, if not crucial, role in the surface enhancement of the electron–phonon interaction and in related properties such as the surface electron lifetimes and the inelastic electron tunneling spectroscopy (IETS). A key step of this recent clarification was the explicit calculation of the adiabatic phonon-induced surface charge density oscillations and related HAS amplitudes [39]. The same microscopic interaction between surface atomic and electronic degrees of freedom also governs thin-film superconductivity and the non-adiabatic processes determining surface electron lifetimes and transport properties. All these aspects concerning surface electron–phonon interactions are thoroughly analyzed in a recent review by Hofmann *et al* [40] and will not be discussed here.

In what follows we shall restrict the discussion to the recent DFPT studies on Al(001) (section 2) and Cu(111) (section 3), the previous studies being thoroughly discussed in the review by Heid and Bohnen. In both cases the surface relaxation modulating the first interlayer distances is responsible for an extended surface perturbation of the dynamical matrix, encompassing at least two more layers beneath the surface, which allows for the appearance of subsurface resonances of optical character and complex hybridization schemes. In this respect these DFPT results have fully validated the previous studies based on the ME and the EA methods, providing these effective semi-empirical methods with a solid first-principles justification. In section 4 the HAS results recently reported for ultrathin films of Pb(111) on Cu(111) are discussed. The facts that He atoms are inelastically scattered by the phonon-induced surface charge density oscillations, and that in free-electron systems like thin Pb films the surface charge density can respond to the motion of atoms deeply buried beneath the surface, account together for the evidence that HAS can measure in thin films many dispersion curves of subsurface phonons, including those propagating at the interface with the substrate. A short comment is devoted to the interesting and not yet fully investigated case of ultrathin magnetic Fe(001) films on Cu(001) in view of future ^{3}He spin-echo scattering measurements.

2. Al(001): subsurface optical modes

Aluminum has been the subject of early studies on the surface phonon dispersion curves in low-index surfaces. Two different sets of HAS measurements have been reported in [29, 30] and [31] for Al(001) in the ⟨110⟩ direction (figures 1(a) and (b), respectively). These data also proved that in a nearly-free-electron sp-bonded metal surface resonances occur in proximity to the bulk longitudinal acoustic edge (L and Z in figure 1), albeit weaker than the ordinary Rayleigh wave (RW). The *ab initio* analysis of the first set of data (figures 1(a) and (c)), carried out by Eguiluz *et al* on the basis of the DR-PPP method [29, 30], accounted for the existence of the longitudinal resonance (L) and of a weaker resonance of shear-vertical polarization (Z). These authors argued that the perturbation shares the complexity of the surface relaxation field and is therefore more extended in depth than originally conjectured on the basis of simple Born–von Kàrmàn force constant (BvK) models [11–13]. The second set of data [31] revealed for Al(001) in the ⟨110⟩ direction another resonance of acoustic nature whose group velocity is unexpectedly 40% larger than the corresponding bulk longitudinal velocity (labeled '2' in figure 1) Although both a semi-empirical BvK model and the DR-PPP calculations apparently also account for this additional feature, the occurrence of this mode represents another puzzle in the surface physics of nearly-free-electron metals. This unclear situation motivated a new study of Al(001) surface dynamics on the basis of DFPT [38].

The complex structure of the surface dynamical matrix argued by Eguiluz *et al* [29, 30] is related to the rearrangement of the surface free-electron charge and the consequent changes

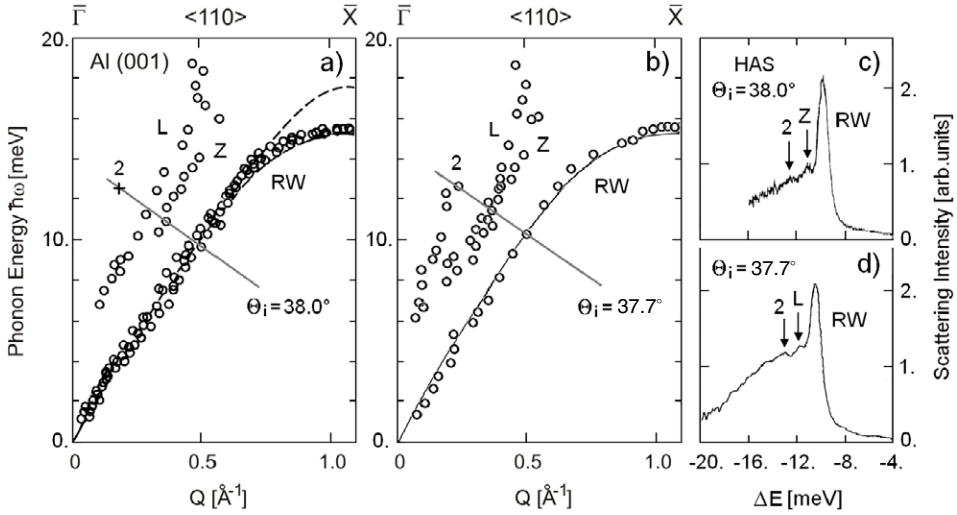

Figure 1. The experimental HAS dispersion curves (○) of surface phonons of Al(001) along the ⟨110⟩ directions and an example of two scattering intensity spectra measured at a given incident angle Θ_i as reported in [30] ((a) and (c)) and [31] ((b) and (d)). Besides the Rayleigh wave (RW), observed up to the Brillouin zone (BZ) boundary ($\bar{X}$ point), the longitudinal acoustic resonance (L) is also observed, though the spectral intensity of the L resonance ((b) and (d)) is much smaller than for the RW. In this respect sp-bonded metals differ from noble and transition metal surfaces where the L mode HAS intensity is comparable or larger than that of RWs. As appears in (a) and (c) the bunch of points labeled Z possibly belong to another resonance of shear-vertical polarization [30]. Moreover both sets of data show another bump corresponding in (b) to a steeper dispersion curve (2). (Adapted from [30, 31].)

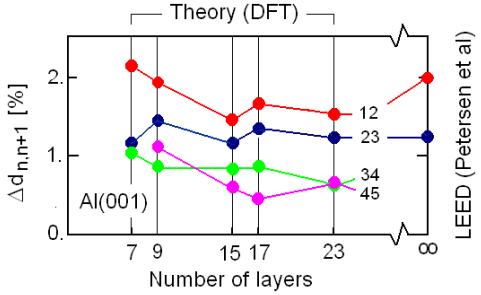

Figure 2. Spacing between the nth and the $(n+1)$th layer for $n = 1$–4 in Al(001) slabs of different thicknesses calculated with DFT [38, 40] and compared to the LEED data ($N = \infty$) of Petersen *et al* [43]. See table 1 for a comparison to FLAPW calculations by da Silva [41] and other LEED data by Berndt *et al* [42].

Table 1. The elastic relaxation of the first four surface interlayer spacings calculated for Al(001) slabs of different thicknesses (expressed in the number of monolayers (ML)). The first-principles calculations based on the full-potential linearized augmented plane wave (FLAPW) method by da Silva [41] and a few available LEED experimental data [42, 43] are also reported for comparison.

Al(001)	Δd_{12} (%)	Δd_{23} (%)	Δd_{34} (%)	Δd_{45} (%)	Reference
7 ML	2.11	1.14	1.01	—	[38]
9 ML	1.93	1.40	0.87	1.06	[38]
15 ML	1.41	1.13	0.83	0.60	[38]
17 ML	1.65	1.30	0.86	0.40	[38]
23 ML	1.50	1.19	0.64	0.66	[38]
FLAPW (9 ML)	1.535	0.432	−0.019	−0.894	[41]
FLAPW (15 ML)	1.600	0.549	0.016	−0.429	[41]
FLAPW (17 ML)	1.598	0.436	−0.020	−0.682	[41]
LEED	1.84	2.04	—	—	[42]
LEED	2.0 ± 0.8	1.2 ± 0.7	—	—	[43]

of the interlayer distances between the first few surface atomic planes [16]. The fact that three to four atomic layers are affected by the surface relaxation implies an extensive change of force constants, certainly not restricted to the topmost surface plane. Thus a prerequisite for an accurate calculation of the surface phonons is a reliable determination of the surface relaxation for as many layers as possible. A well-equilibrated surface is a necessary condition for the dynamical matrix to fulfill the rotational invariance and stress-free conditions [5].

The relaxation of the interlayer spacing for the first four surface layers of Al(001) has been calculated with density functional theory (DFT) for five different slab thicknesses (figure 2) [38]. The results are compared in table 1 with other calculations based on the full-potential linearized augmented plane wave (FLAPW) method [41] and with the available LEED experimental data [42, 43]. The dependence on the slab thickness shows in all cases an oscillatory behavior with a slow convergence to the thick-slab limit. The first interlayer spacing Δd_{12} calculated with DFT agrees with the FLAPW result, whereas the relaxations between inner planes are found to be substantially larger than the FLAPW ones and all positive. It is noted, however, that the DFT results are in better agreement with the more recent LEED data by Petersen *et al* [43], though the latter are affected by a large experimental error and are only available for the first two spacings.

The surface dynamics of Al(001) has been calculated for the equilibrated slabs of $N_L = 7$ and 17 layers [40, 38] by means of the DFPT [37]. Ultrasoft pseudopotentials have been used together with the generalized gradient approximation (GGA) and the correlation energy functional introduced by Perdew *et al* [44]. Further details are in [38]. An important aspect of this DFPT calculation for the 17-layer slab is

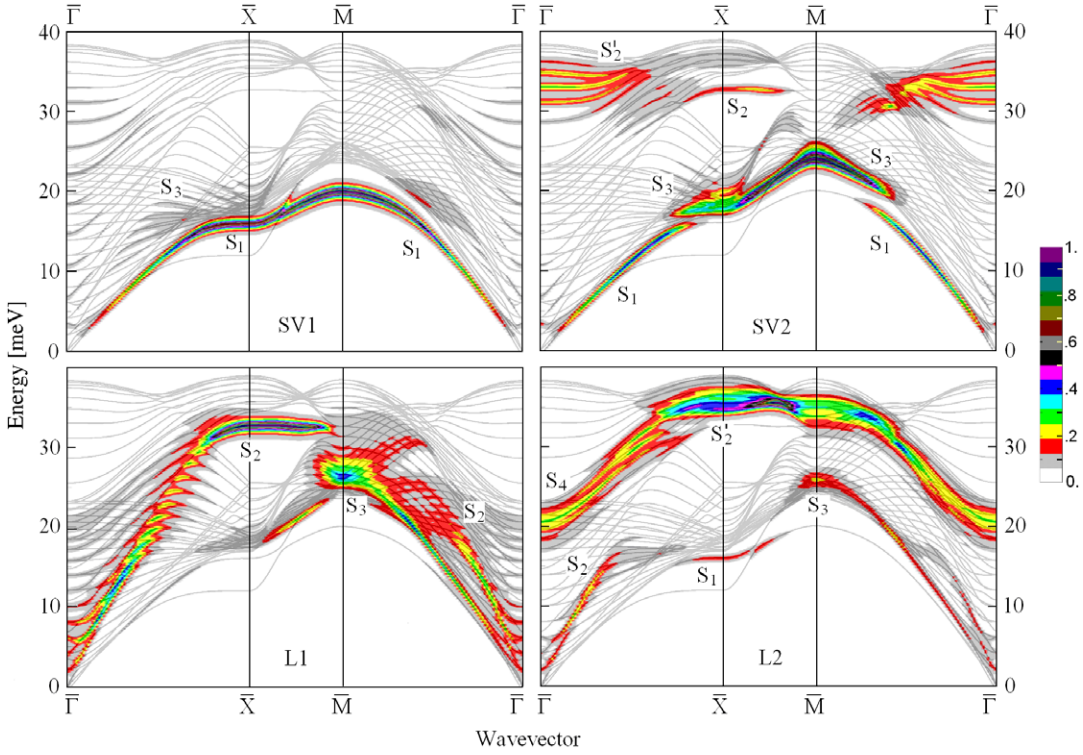

Figure 3. Contour plots of the spectral intensities of the shear-vertical (SV1, SV2) and longitudinal (L1, L2) components of the surface modes and resonances of Al(001) projected onto the first (SV1, L1) and second (SV2, L2) surface layer. The DFPT calculation has been performed for a 17-layer slab. The width of the S'_2 resonance is larger than the separation of the bulk dispersion curves and appears to be spread over several bulk lines. The gray (color online) scale is given on the right.

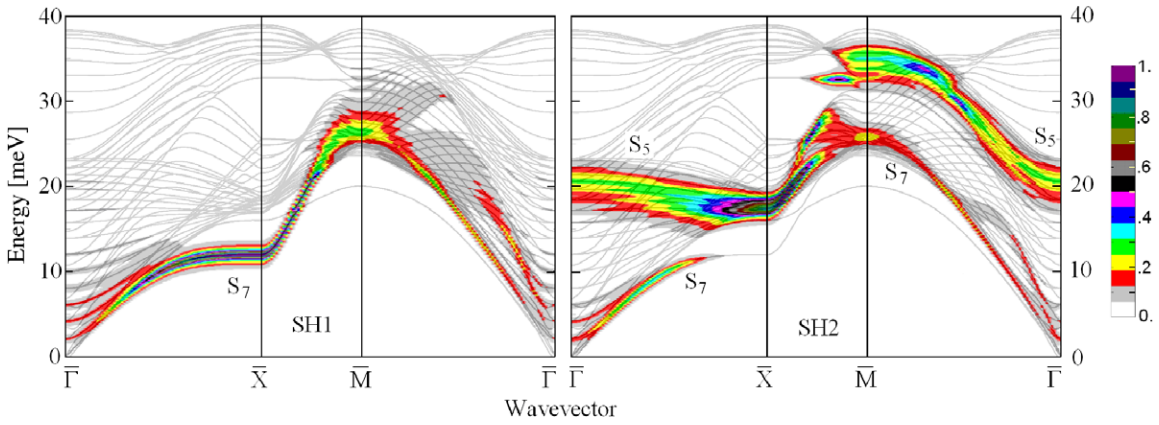

Figure 4. Same as figure 3 for the shear-horizontal components projected onto the first (SH1) and second (SH2) surface layer.

that the full dynamical matrix has been generated without resorting to the insertion of bulk layers into a thinner slab with surface force constants in order to reduce the computational weight. The bulk-into-slab insertion procedure, which has been frequently used in previous *ab initio* calculations [32], might be questionable due to the intrinsic extension of the surface perturbation, which may span several layers, and to possible violations of the rotational invariance conditions in the bulk-to-surface matching region. This aspect is further discussed below for the Cu(111) case.

The phonon dispersion curves of Al(001) calculated by Chis *et al* [38] with the DFPT for a slab of 17 layers are collected in figures 3 and 4. They are plotted together with the spectral intensities of the surface modes, projected onto the first and second surface layer for the sagittal components (shear-vertical SV1 and SV2, and longitudinal L1 and L2, respectively) (figure 3) and for the shear-horizontal (SH1, SH2) components (figure 4): their contour plots are mapped in a color scale, increasing from gray to red to violet, on top of the dispersion curves.

A detailed comparison between the HAS data reproduced in figure 1(a) and the sagittal components of the acoustic surface branches in the first and second layer is shown in figure 5. The Rayleigh wave branch (S_1) shows, as expected,

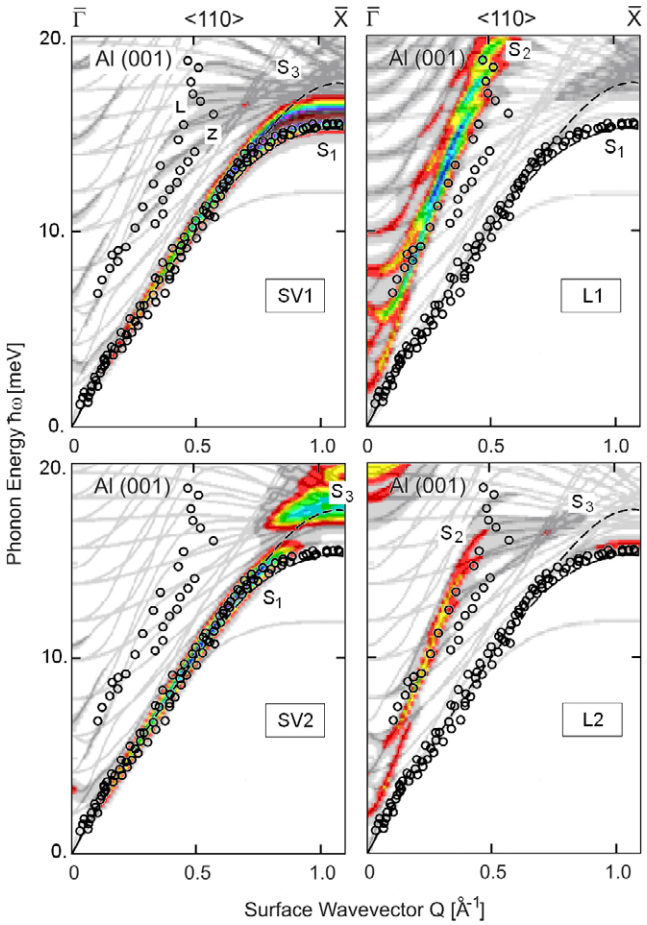

Figure 5. Comparison of the HAS data (○) from [30] with the calculated SV and L surface phonon dispersion curves and their amplitudes (color code as in figures 4–6) projected onto the first (SV1, L1) and second (SV2, L2) layer in the ⟨110⟩ direction.

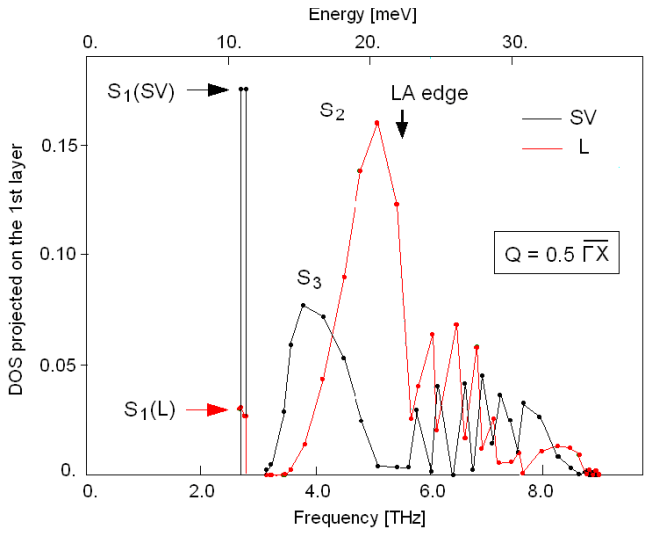

Figure 6. Densities of phonon states of shear-vertical (SV, black line) and longitudinal (L, red line) polarization projected onto the first surface layer at one-half of the $\bar{\Gamma}\bar{X}$ direction for the 17-layer Al(001) slab derived from the DFPT calculation of [38]. The peak corresponding to the Rayleigh wave (RW) has 7/8 of SV character and 1/8 of L character due to its elliptical polarization in the sagittal plane. The S_2 and S_3 broad features correspond to the resonances observed with HAS by Gaspar *et al* [30].

a large SV intensity in the first layer (SV1), which increases towards the zone boundaries due to the increasing localization. In fact, its second-layer intensity (SV2) decreases at larger wavevectors, part of its amplitude at $\bar{X}$ being transferred to the longitudinal component (L2) and part to the upper S_3 resonance, which therefore is classified as a second-layer zone-boundary SV resonance. However, the S_3 resonance shows also some intensity in the first layer as both an SV (SV1) and an L (L1) resonance and is weakly hybridized with the S_2 resonance in the second layer (L2). Thus the set of experimental HAS data attributed by Gaspar *et al* [30] to a *z*-polarized resonance (marked Z in figure 1(a)) can indeed be associated with a continuation of the S_3 resonance. Unfortunately the *z*-polarized resonance has not been detected with HAS up to the zone boundary, due to the HAS intensity cutoff at large wavevector transfers [45].

The experimental L-polarized resonance branch (figures 1(a) and (b)) is very well reproduced by the DFPT calculation, which shows a strong resonance in the first layer along the LA edge (S_2 in figure 3 (L1)). The L resonance is also visible in the second layer (L2) up to about one-half of the zone, then fades out due to the hybridization with the SV S_3 resonance mentioned above. A plot of the calculated density of states (DOS) for the SV and L components projected on the first surface plane for the surface wavevector Q at one-half of the zone in the $\bar{\Gamma}\bar{X}$ direction (figure 6) shows indeed that both the stronger S_2 and weaker S_3 resonances are rather broad, and the latter is partly covered by the former so as to make them hard to resolve despite the comparatively good resolution of HAS spectroscopy. It is also noted from figure 3 (L1) that the Rayleigh waves (S_1) have a negligible L component in the first layer. As seen in figure 6 they have indeed an elliptical polarization in the sagittal plane, but the corresponding peak has a SV character for about 7/8 of its total amplitude and an L character for 1/8 of its amplitude. Altogether the DFPT calculation accounts very well for the observed acoustic resonances and confirms the original DR analysis by Gaspar *et al* [30] as regards the nature of the so-called anomalous longitudinal resonance. It is unfortunate that such a comparison is not possible for the $\bar{\Gamma}\bar{M}$ direction, for which no HAS data are available.

Besides the acoustic resonances, the DFPT calculation predicts strong, albeit broad, resonances of optical nature, all localized in the second layer: the broadest one has an SV polarization and the highest energy (S_2'); the other two with L and SH polarizations (S_4 and S_5, respectively) are comparatively sharper and degenerate at the zone center. Normally optical surface phonon branches only occur for diatomic crystals, where they are associated with the internal degrees of freedom of the unit cell, just like the bulk optical modes. Thus the occurrence in monoatomic metals of surface optical resonances is a rather interesting novelty. Their localization on the second layer naturally suggests associating them with the important surface relaxation, which yields a sizable change of the interlayer distance between the first two layers with respect to the bulk (table 1).

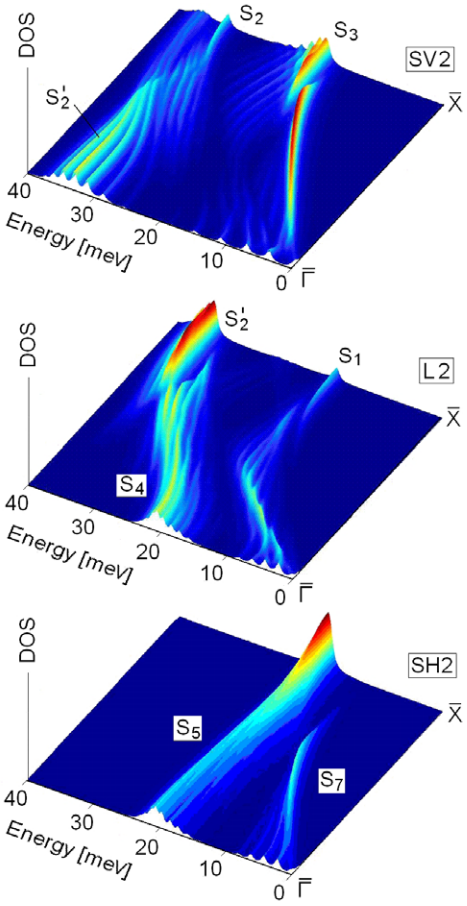

Figure 7. The optical phonon branches of Al(001) S'_2, S_4 and S_5 from a DFPT calculation of the phonon densities of states projected onto the second surface layer for shear-vertical (SV2), longitudinal (L2) and shear-horizontal (SH2) polarizations, respectively, along the $\bar{\Gamma}\bar{X}$ wavevector direction. Unlike the SH S_5 branch, which shows no dispersion up to the zone boundary, where it reaches its maximum amplitude, the optical branches for the SV and L polarizations display strong avoided crossing hybridizations with the acoustical branches and each other. The degenerate pair of optical resonances S_4 and S_5 at the zone center are an example of Lucas optical surface modes, so far only known in cubic diatomic crystals [46], whereas the S'_2 resonance corresponds to the SV optical mode predicted by Wallis also in diatomic crystals [47].

The amplitudes of the optical surface resonances are better seen in the phonon densities of states projected onto the second surface layer for shear-vertical (SV2), longitudinal (L2) and shear-horizontal (SH2) polarizations, along the $\bar{\Gamma}\bar{X}$ wavevector direction (figure 7). Unlike the SH S_5 branch, which shows no dispersion up to the zone boundary, where it reaches its maximum amplitude, the optical branches for SV and L polarizations display strong avoided crossing hybridizations with the acoustical branches and each other. The analogy with the surface optical branches in diatomic crystals is further appreciated in the degenerate pair of optical resonances S_4 and S_5 at the zone center, which have been predicted long ago by Lucas for cubic diatomic insulators [46], and are therefore termed Lucas modes [5, 47]. Similarly the S'_2 resonance corresponds to the SV optical surface mode predicted even earlier by Wallis, also in diatomic crystals (Wallis mode, [5, 48]).

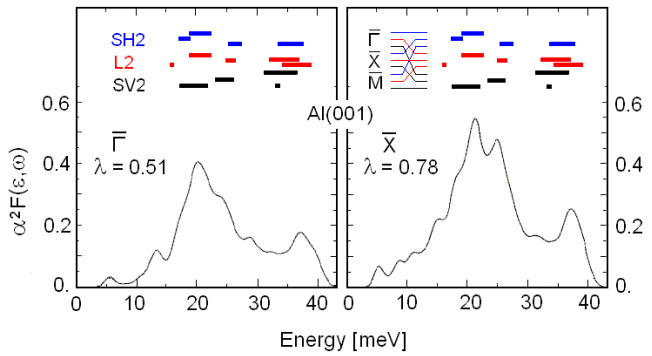

Figure 8. The Eliashberg electron–phonon coupling function and the related electron–phonon parameter λ calculated by Chulkov *et al* [49] for the electronic surface states of Al(001) at $\bar{\Gamma}$ and $\bar{X}$: the main peaks of $\alpha^2F(\varepsilon_F, \omega)$ approximately correspond to the positions of the second-layer surface optical phonon resonances at the symmetry points $\bar{\Gamma}$, $\bar{X}$ and for $\bar{M}$ (cf figures 4–6), here represented for the three polarizations SH, L and SV by blue, red and black bars, respectively (insets), whose length gives the corresponding resonance full width at half-maximum (FWHM).

Optical surface modes are likely to play an important role in the surface electron–phonon interaction, as it may be argued from the Eliashberg electron–phonon coupling function $\alpha^2F(\varepsilon_F, \omega)$ calculated by Chulkov *et al* [49] for the $\bar{\Gamma}$- and $\bar{X}$-point surface state electrons in Al(001). From a comparison with the DFPT surface phonon dispersion curves shown in figures 3, 4 and 7 it appears that for both $\bar{\Gamma}$ and $\bar{X}$ symmetry points the main features of $\alpha^2F(\varepsilon_F, \omega)$ found at 37 meV and above 20 meV can be associated with the flat branches S'_2 in SV2, S_5 in SH2 and also with the dispersed optical branch S_4 in L2. This can be appreciated in figure 8, where $\alpha^2F(\varepsilon_F, \omega)$ is compared to the positions and width (FWHM) of the second-layer surface optical phonon resonances at the symmetry points $\bar{\Gamma}$, $\bar{X}$ and $\bar{M}$ for the three polarizations SH, L and SV (cf figures 3 and 4). A similar correspondence between the inelastic electron tunneling spectroscopy (IETS) features and the second-layer optical phonon resonances shall be discussed for Cu(111) in section 3.

The second set of HAS data reported by Franchini *et al* [31] (figure 1(b)) deserves some comment. It shows, besides the *x*- and *z*-polarized branches (now unresolved), a steep branch, labeled by '2', which clearly does not correspond to any feature of the calculated DFPT surface phonon dispersion curves (figure 9(a)). When compared to the calculated dispersion curves for L polarization, the '2' branch appears to be much steeper than both the calculated and measured L-polarized branches. Note that a similar branch has been observed with HAS in Cu(001) along the ⟨100⟩ direction [26]: two typical HAS spectra are shown in figure 9(b). As compared to Al(001) (figures 1(c) and (d)), the HAS scattering intensity from the L mode of Cu(001) is much stronger than that from the RW, whereas the peak associated with the '2' resonance is only slightly more evident than that seen in Al(001). As discussed in [26], the maximum labeled by '2' is believed to be associated with the multiphonon background, though the latter (broken line in figure 11(b)) is actually much broader than the '2' peak. The location of the '2' resonance in Cu(001) is also

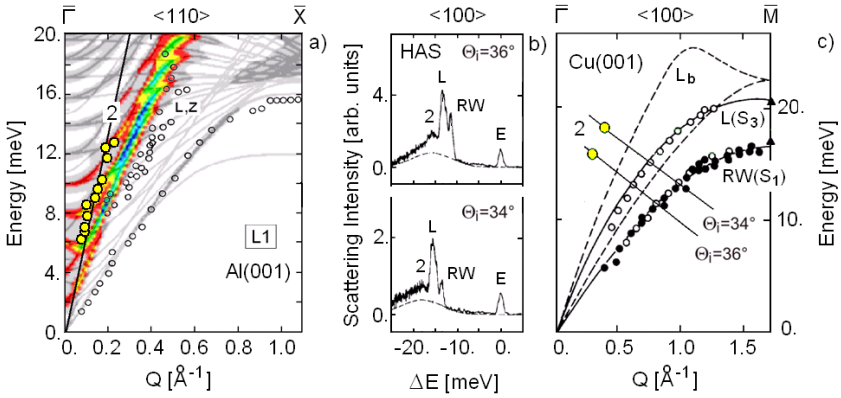

Figure 9. (a) The dispersion curve of the resonance '2' (large open circles) measured in Al(001) along the ⟨110⟩ direction by Franchini *et al* [31], when compared to the calculated dispersion curves for L polarization, appears to be much steeper than the calculated (gray (color online)) and measured L-polarized branches. A similar branch has been observed with HAS in Cu(001) along the ⟨100⟩ direction [26]: two typical HAS spectra are shown in (b) for incident angles $\Theta = 34°$ and 36° with the corresponding scan curves and data points in the momentum–energy plane plotted in (c). As compared to figures 1(c) and (d), in Cu(001) the scattering from the L (S_3) mode is much stronger than from the RW (S_1), whereas the peak associated with the '2' resonance is comparable to that of Al(001). The '2' resonance is believed to be associated with the multiphonon background (broken lines in (b)), though the latter is much broader than the '2' peak. (c) Also in Cu(001) the '2' resonance (large open circles) is well above the L bulk edge (L_b) and the experimental L (S_3) resonance.

well above the L bulk edge (figure 9(c), large open circles) and the experimental L resonance (S_3) as in Al(001). Also this steep branch, as far as it is related to a single surface excitation, seems to be a common feature to a number of surface metals, like the long discussed longitudinal acoustic resonance.

Since He atoms do not interact with the atomic displacements directly but through the displacement-induced surface charge density oscillations, it has been argued that HAS should also be sensitive to low-energy surface collective excitations like acoustic plasmons, though with a comparatively lower intensity and essentially zero parallel momentum transfer as compared to Rayleigh waves [50]. The finding of surface optical phonon resonances is, however, complicating the scenario, since acoustic plasmons are predicted to hybridize with surface optical phonons (*plasmarons* [51]). So far the only measurements of the surface acoustic plasmon dispersion on metal surfaces have been achieved with EELS [52, 53] as a realization of previous theoretical predictions [54, 55], whereas no evidence has been obtained yet for inelastic HAS from surface acoustic plasmons. The subject is certainly worth being investigated, however, since the surface plasmon dispersion law in the zero-momentum limit and its mixing with the phonon branches bear important information about the nature of electronic surface states, their band structure and their interaction with phonons, all this falling in an energy domain which is presently inaccessible to EELS.

3. Cu(111): phonon-induced surface charge density oscillations

Although the low-index surfaces of copper are the most thoroughly investigated among all metal surfaces from the point of view of surface dynamics [5], only recently has the intrinsic nature of the surface acoustic resonance observed with HAS been fully elucidated [39]. This result has been obtained through a DFPT calculation of the surface charge density oscillations (CDOs) adiabatically produced by the atomic displacements of any given surface phonon. The evaluation of the CDOs down to the range of 10^{-6} au has allowed us to estimate the actual inelastic HAS cross section at the experimental incident energies, thus proving that the acoustic longitudinal resonance is not an artifact of HAS due to the peculiarity of the He–phonon interaction discussed above, but an intrinsic feature of metal surface dynamics. This is quite intriguing, however, since the displacement field of this resonance is, to a large extent, subsurface, due to the hybridization with an optical surface resonance. This conclusion, besides solving the Bortolani–Mills paradox, provides a solid basis to some previous semi-empirical approaches such as the EAM and the ME method, which had correctly pinpointed the origin of the subsurface resonance and its HAS amplitude, respectively. It should be mentioned that a DFPT calculation of the surface phonon dispersion curves of Cu(111) was first reported by Heid and Bohnen [36]. However, neither this calculation nor the previous DFPT analysis of Cu(001) by Dal Corso [56] have considered the problem of the L resonance, though in the latter case its HAS amplitude is much larger than that of the RW (figure 9(b)).

The DFPT study by Chis *et al* [39] here discussed was based on ultrasoft pseudopotentials and a generalized gradient corrected (GGA) exchange and correlation energy functional, according to Perdew, Burke and Ernzerhof (PBE) [44]. A plane wave basis with a 30 Ryd energy cutoff for the wavefunctions and 480 Ryd for the charge density has been used. The relaxations at equilibrium of the first two interlayer spacings Δd_{12} and Δd_{23} have been calculated for a 7-layer and an 18-layer slab (table 2). The values of Δd_{12} are about the same for the two slabs and agree within the experimental error with the experimental medium-energy ion scattering (MEIS) [57] and low-energy electron diffraction (LEED)

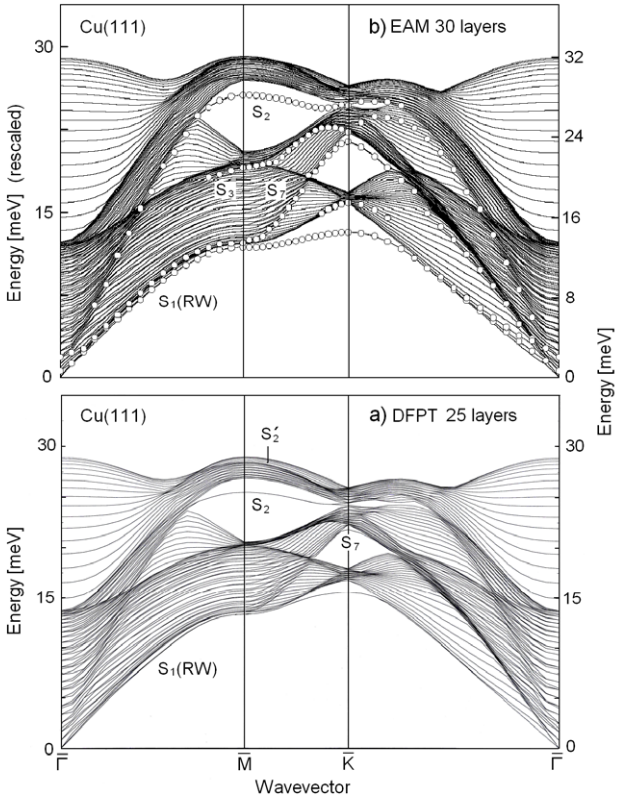

Figure 10. (a) DFPT calculation of the surface phonon dispersion curves of a 25-layer slab of Cu(111) [39]. (b) The set of surface phonon dispersion curves obtained from DFPT is well reproduced by a semi-empirical calculation for a 30-layer slab based on the embedded-atom method (EAM) (open circles) [23]. The latter is plotted in its original energy scale (right-hand ordinate scale) and rescaled by about 10% (left-hand ordinate scale) so as to match the DFPT maximum phonon energy. The analysis of EAM eigenvectors made it possible to identify some surface resonances such as S_7 and the long discussed S_3.

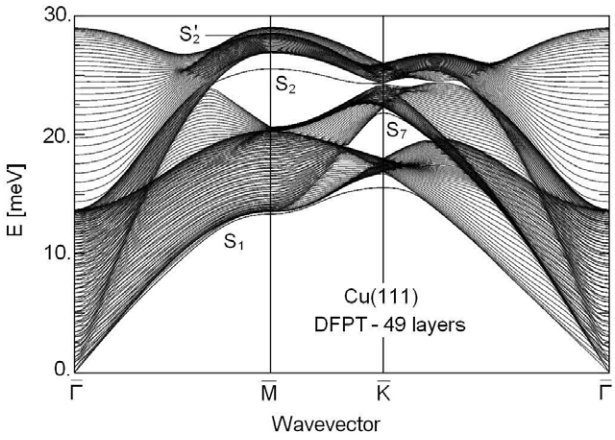

Figure 11. Surface phonon dispersion curves of a Cu(111) slab of 49 atomic layers calculated with DFPT [39].

Table 2. DFPT calculated interlayer distances of 7-layer and 18-layer Cu(111) slabs compared with medium-energy ion scattering (MEIS) and low-energy electron diffraction (LEED) data and with other *ab initio* calculations.

Cu(111)	Δd_{12} (%)	Δd_{23} (%)	Reference
DFPT 7 ML	-1.195	-0.487	[40]
DFPT 18 ML	-1.183	-0.821	[39]
Other *ab initio*	-0.9	—	[59, 60]
methods	-1.58	-0.73	[61]
EAM	-1.14	—	[62]
	-1.05	-0.07	[23]
MEIS	-1.0 ± 0.4	-0.2 ± 0.4	[57]
LEED	-0.7 ± 0.5	—	[58]

data [58], and are consistent, within the expected numerical uncertainty, with previous *ab initio* [59–61] and semi-empirical calculations [23, 62]. The DFPT values of Δd_{23} show a large change with the layer thickness, which makes the comparison with the MEIS datum and the quite disperse results of other theoretical methods less significant (table 2).

The dynamical matrix of the equilibrated slab has been constructed by calculating the interatomic force constants for bulk Cu and for the 7-layer Cu(111) slab. Then the N-layer slab has been obtained with the current procedure of replacing the central layer of the 7-layer slab with a set of $N - 6$ bulk layers (*insertion procedure*). Care was taken to ensure that force constants fulfill rotational invariance conditions [5] in the matching regions. The radial force constant between nearest neighbors on the surface plane was found to be 11% softer than that in the bulk. The calculations here reproduced are for $N = 25$ (figure 10(a)). In order to assess the reliability of the approximation based on the insertion of bulk planes, Chis *et al* performed for comparison a calculation for the pure 18-layer slab, with no insertion of bulk planes. The resulting dispersion curves and phonon DOSs are substantially the same as for the 25-layer slab obtained from the 7-layer slab with the insertion procedure. On the other hand the calculation for 49 layers generated with the insertion procedure (figure 11) showed no change in the surface branches with respect to the 25-layer slab, which ensured a good convergence already at 25 layers. It is worth noting that the set of surface phonon dispersion curves obtained from DFPT are well reproduced by a semi-empirical calculation for a 30-layer slab based on the embedded-atom method (EAM) [23] (figure 10(b)), apart from a 10% rescaling by about 10% (figure 10(b), left-hand ordinate scale). Moreover the analysis of EAM eigenvectors allowed us to identify some surface resonances such as S_7 and the long discussed S_3. This qualifies EAM as an expedient tool for a fast and reliable, albeit semi-empirical, analysis of metal surface dynamics, especially for extended surface cells [23] which would require a large computational effort with DFPT.

The densities of surface phonon states projected on the first and second surface layers of a Cu(111) 25-layer slab calculated with DFPT along the $\bar{\Gamma}\bar{\mathrm{M}}$ direction are shown in figure 12 for the shear-vertical (SV1, SV2), longitudinal (L1, L2) and shear-horizontal (SH1, SH2) polarizations. Similarly figure 13 displays the DOSs projected onto the first and second surface layers for the $\bar{\Gamma}\bar{\mathrm{K}}$ direction. There are some similarities with the DOSs of Al(001) (cf figures 3, 4 and 7). Also in Cu(111) the DOSs projected onto the second layer exhibit intense resonances of optical character (SV2, L2 and SH2 in figures 12 and 13). With respect to Al(001), the large S_3 resonance at the zone boundary of SV2 is here clearly detached

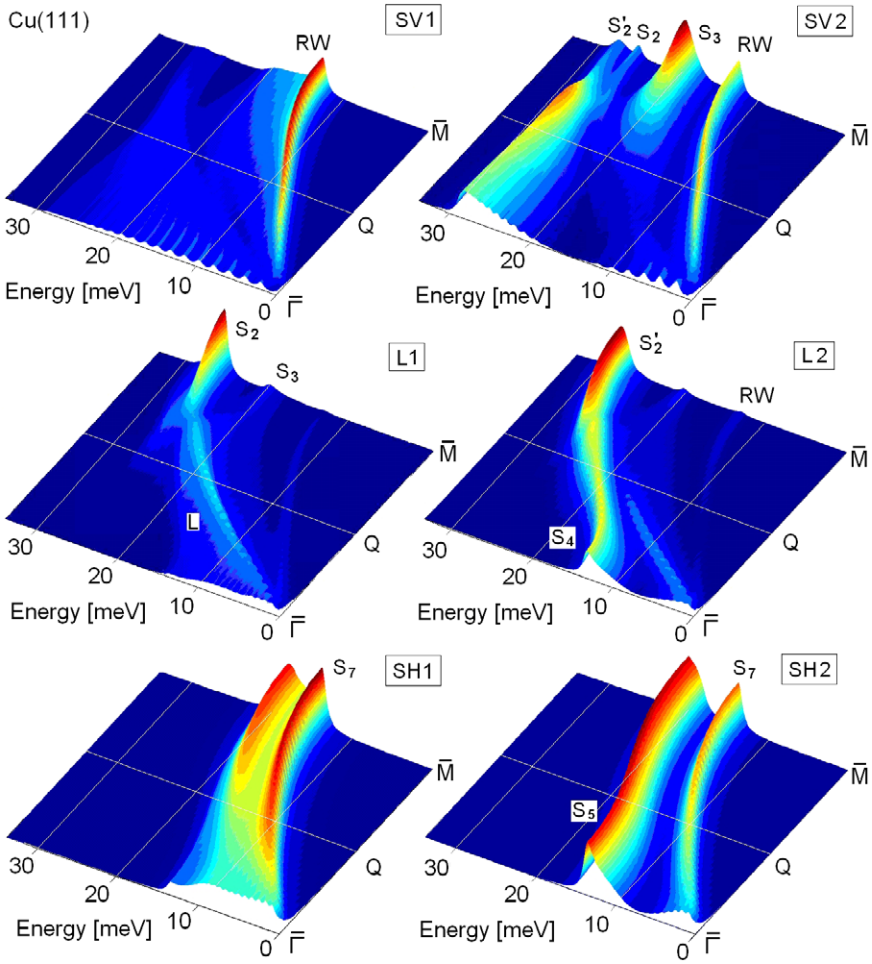

Figure 12. The densities of surface phonon states for a Cu(111) 25-layer slab along the $\bar{\Gamma}\bar{M}$ direction calculated with DFPT projected onto the first and second surface layers for the sagittal polarizations SV (SV1, SV2) and L (L1, L2), and for the shear-horizontal polarizations (SH1, SH2) (arbitrary units).

from the RW at the $\bar{M}$ point and receives most of its large intensity from the avoided crossing with the large and broad optical resonance S_2. Moreover the SH optical resonance S_5 (figures 12 and 13, SH2) is not dispersionless as in Al(001) (figure 7) but exhibits an avoided crossing with the acoustic S_7 branch, acquiring an upward dispersion. However, also for the Cu(111) the Lucas mode pair (S_4, S_5) is degenerate at $\bar{\Gamma}$ by symmetry.

The ridges of the projected DOSs allow us to construct the dispersion curves of all the surface localized and resonant surface phonon branches. They are collected in figure 14 for the $\bar{\Gamma}\bar{M}$ direction and compared with the data points derived from HAS [39, 2] and EELS [7, 8] experiments (black and red symbols, respectively). The full lines, corresponding to the DOS ridges, are labeled as in figure 11; the broken lines describe the would-be dispersion curves in the absence of avoided crossings. There is a large avoided crossing and consequent exchange of polarization between SV1 and L1 branches, which fully accounts for the conversion at $Q \sim 0.8$ Å^{-1} of the acoustical first-layer L resonance into the second-layer SV resonance S_3. The agreement of the DFPT calculation with the HAS and EELS data is very good over all spectral regions. The new HAS data reported in [39] have also provided the first experimental evidence for the optical L2 (S_2') resonance.

The SV2–L1 avoided crossing is well reflected in both HAS and EELS data, which follow the L branch up to one-half of the zone, then deviate towards the S_3 resonance, which has only a weak L component in the first and second layer but an SV component in the second layer rapidly growing towards the $\bar{M}$ point. The origin of such intensity transfer from the L to the S_3 mode, originally interpreted as a dramatic softening of the L resonance, is well understood for EELS, since electrons penetrate sufficiently to probe the second-layer SV displacements. In contrast this poses a problem for HAS since He atoms do not penetrate at all. Although the hybridization mechanism was clearly established by former calculations with the EAM [19, 20], effective-medium [63, 64] and first-principles frozen-phonon [65, 66] methods, the HAS puzzle received no convincing explanation.

The one-phonon HAS differential reflection coefficient in the eikonal approximation [67] is expressed, at $T = 0$ and up to kinematic factors, by

$$\frac{\mathrm{d}^2\Re^{(1)}}{\mathrm{d}E_\mathrm{f}\,\mathrm{d}\Omega_\mathrm{f}} \propto \sum_{Q\lambda} |\Delta\zeta_\lambda(Q,\zeta_\mathrm{t})|^2 \delta(E_\mathrm{i} - E_\mathrm{f} - E_\lambda). \qquad (1)$$

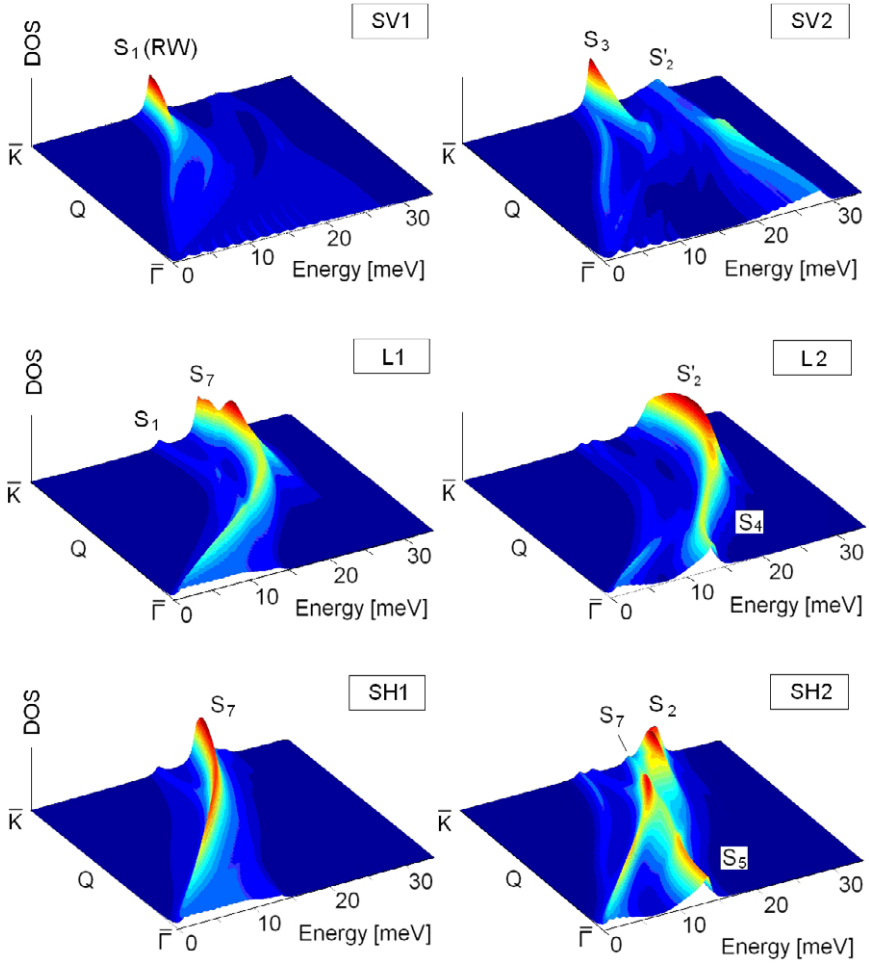

Figure 13. Same as figure 11 for the $\bar{\Gamma}\bar{\mathrm{K}}$ direction (arbitrary units).

Here $\Delta\zeta_\lambda(Q, \zeta_t)$ is the 2D Fourier transform of the dynamic surface corrugation $\Delta\zeta_\lambda(R, \zeta_t)$ induced by the λth phonon at position (R, ζ_t), where R is the position on the surface plane and $\zeta_t = \zeta_t(R)$ is the distance from the surface plane of the classical He–surface potential turning point for an He atom incident energy E_i. E_λ is the phonon energy and E_f the final energy of the scattered He atom. In a first approximation the dynamic corrugation can be derived from the dependence of the surface charge density $n(R, \zeta)$ on the normal coordinate ζ as obtained from DFPT. For Cu(111) this turns out to be a pure exponential [39]

$$n(R, \zeta) = n_t \exp[-\beta(\zeta - \zeta_t)], \tag{2}$$

with $\beta = 2.79$ Å^{-1} and

$$n_t = E_i \cos^2\theta_i/(364eVa_0^3) \tag{3}$$

the static charge density at the turning point for an incident angle θ_i. The constant in equation (3) (with a_0 the Bohr radius) is that of the Esbjerg–Nørskov potential [68] as given by Cole and Toigo [69]. Thus the dynamic corrugation associated with the λth phonon is simply proportional to the surface CDO $\Delta n_\lambda(R, \zeta)$, i.e.

$$\Delta\zeta_\lambda(R, \zeta_t) \cong \Delta n_\lambda(R, \zeta_t)/\beta n_t. \tag{4}$$

In this way the calculation of the inelastic HAS amplitude is reduced to that of the surface CDO for each phonon. Examples of surface CDOs induced by a selection of surface localized phonons and resonances with sagittal polarization are shown in figure 15 at some special points of the Brillouin zone [39][6]. The contour lines for positive (red online) and negative (blue online) surface CDOs are plotted for values of $\Delta n_\lambda(R, \zeta)$ equal to $2^{-k} \times 10^{-4}$ au and $-2^{-k} \times 10^{-4}$ au, respectively, with $k = 0, 1, 2, \ldots, 7$. The almost uniform separation of the contour lines far away from the surface plane indicates an exponential decay of the dynamic CDO as well. It appears that at distances of about 3 Å away from the surface plane, where He atoms at thermal energies are repelled, the CDOs of the S_3 resonance and of the RW at the $\bar{\mathrm{M}}$ point are comparable, despite the fact that the largest S_3 amplitude is in the second layer.

The highest subsurface optical resonance SV2($\bar{\Gamma}$) yields appreciable, albeit uniform, CDOs, although no HAS signal has been reported in past experiments from this branch due to the use of a comparatively low incident energy and to the cutoff occurring at large energy transfers [5, 67]. It is interesting to note that the CDO has the signature of the large second-layer atom displacements rather than of the much

[6] In figure 3 of [39] the CDOs at $\bar{\mathrm{M}}/2$ have been misattributed to the $\bar{\mathrm{M}}$ point. An erratum with the right figure is to appear.

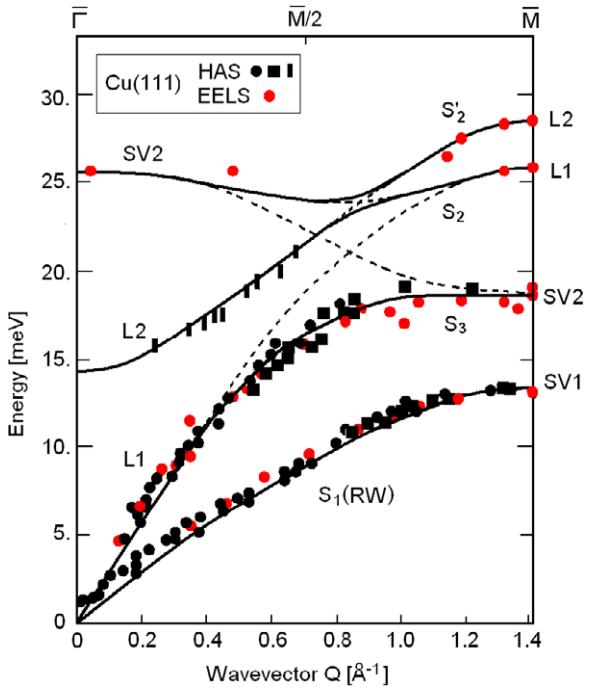

Figure 14. The ridges (full lines) of the surface phonon DOSs of Cu(111) calculated with DFPT for the first- and second-layer sagittal polarizations SV1, SV2, L1 and L2 in the $\bar{\Gamma}\bar{\mathrm{M}}$ direction (cf figure 11) are compared with the experimental HAS (black symbols [39]) and EELS data (gray (red online) symbols [7–9]). The strong hybridization between the longitudinal acoustic resonance in the first layer (L1) and the optical SV resonance in the second layer (SV2) (broken lines) leads to a large avoided crossing. In this way the acoustic longitudinal resonance S_3 acquires beyond 2/3 of the zone an SV character with a larger amplitude in the second layer. Another smaller avoided crossing occurs between S_2 and S_2' so that the L2 resonance gradually evolves into L1 ending as a surface localized gap mode.

smaller, 180° out-of-phase first-layer atom displacements: when the first interlayer distance contracts (extends) the charge is squeezed out (in) the interlayer region. More interesting is the optical longitudinal resonance, which at the zone center (L2($\bar{\Gamma}$)) has its larger displacement in the second layer and is longitudinal, so that its CDO is negligible already at 2 Å above the surface plane. However, at shorter wavelengths, due to the hybridization with L1 (figure 14), it acquires a surface character transforming at the zone boundary into the surface localized mode $S_2(\bar{\mathrm{M}})$. Despite its perfectly longitudinal character, the associated CDO is comparable to that of $S_3(\bar{\mathrm{M}})$, which can explain the new HAS data aligned on the L2 branch above 0.3 $\mathrm{Å}^{-1}$ (figure 14, ▮). A CDO produced by a purely longitudinal motion of the first-layer atoms has a dominant *quadrupolar* character, whereas the rigid up and down CDO produced in SV2($\bar{\Gamma}$) by the vertical motion of the second-layer atoms has a prevalent *dipolar* character. Figure 15 also shows the CDO associated with the optical SH resonance at the zone center SH2($\bar{\Gamma}$), whose displacements are normal to the (χ, ς) plane, have opposite signs $(+, -)$ and are larger in the second layer. For this mode the surface CDO is even smaller than for L2($\bar{\Gamma}$) and totally negligible.

The CDO calculation elucidated the mechanism for the intense HAS amplitudes from subsurface phonons: the surface charge density has a large susceptibility for certain subsurface phonons or, in other words, the surface electrons are strongly coupled to some subsurface phonons. The semi-empirical ME model [24] actually suggested that the atomic motion in the topmost layers yields mechanical displacements and deformations of the surface charge density of dipolar and quadrupolar character, respectively. This approach, in its phenomenological version known as the pseudo-charge (PC) model, allowed for an excellent fit of the inelastic HAS spectra observed in Cu(001) and Cu(111) [25, 26]. Phenomenological models with a good microscopic basis often help understand specific mechanisms hard to visualize in a first-principles calculation. In the specific case of copper an important conclusion of the PC model analysis was that the non-central forces, accounting for the deviation from the Cauchy relation, and their surface perturbation mostly originate from the quadrupolar terms [5, 25].

The favorable comparison between DFPT and the previous semi-empirical EAM and ME methods is summarized in figure 16. As appears in the first column of figure 16, the first-layer phonon sagittal DOS (SV1 + L1) calculated in the $\bar{\Gamma}\bar{\mathrm{M}}$ direction of Cu(111) with either the EAM [20] or the ME method [25] compare very well with each other and with the corresponding first-principles DOS calculated with DFPT [39]. A similar good agreement is found between the second-layer DOSs for SV polarization between EAM and DFPT calculations (figure 16, second column), thus showing the ability of EAM to predict the surface optical branches and their hybridization schemes. Also the phonon DOS projected onto the dipolar (D1) and quadrupolar (Q1) components of the first-layer charge density oscillation (CDO) obtained with the ME method [25] compares very well with both EAM and DFPT DOSs for SV modes in the second layer. This shows that, in agreement with the DFPT results of figure 15, the surface CDO reflects the SV motion of the underlying second-layer atoms, thus explaining the sensitivity of HAS to subsurface resonances.

The phonon-induced surface CDOs also provides a coupling mechanism for inelastic electron tunneling spectroscopy (IETS). As shown by Lorente and Persson [70], the IETS differential conductivity as measured with a scanning tunneling microscope is proportional to the squared phonon-induced modulation of the surface electron density at the tip apex. Thus any surface phonon producing a large surface CDO should strongly contribute to IETS, whether the atomic displacement is the largest in the surface or in a subsurface layer. In this respect IETS, albeit not momentum-resolved, has something in common with inelastic HAS spectroscopy. Gawronski *et al* [71] were indeed able to obtain images of phonon excitations in Cu(111) and Au(111) by means of STM-IETS. The images show with atomic resolution the surface lattice structure as an effect of surface phonon excitations. The authors argue that modulation of the signal on the atomic scale is related to corresponding variations in the phonon excitation probability. Since the squared CDO associated with a surface phonon at the $\bar{\mathrm{M}}$ point forms a pattern with the period of the surface lattice, the probability of exciting an $\bar{\mathrm{M}}$-point phonon should reflect the lattice structure with atomic resolution, provided its associated

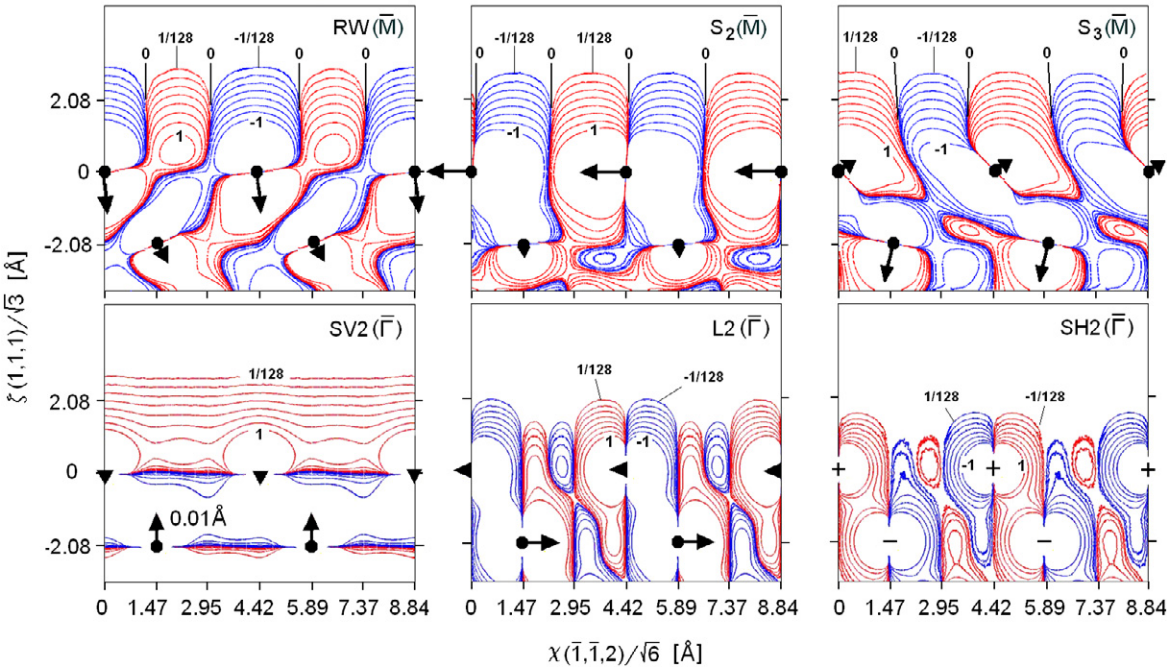

Figure 15. Surface charge density oscillation (CDO) (in units of 10^{-4} au) induced by frozen-phonon displacements (arrows) for the Rayleigh wave, the subsurface optical resonances SV2 ad L2 (S_2) and the surface resonance S_3 at the $\bar{M}$ and $\bar{\Gamma}$ points [39] (see footnote 6). All atomic displacements, except SH2($\bar{\Gamma}$) lie in the sagittal plane (χ, ζ) and have the direction and size of the arrows, the length scale of 0.01 Å being provided by the second-layer displacement of the SV2($\bar{\Gamma}$) mode. The atom displacements of the SH resonance at the zone center, SH2($\bar{\Gamma}$), are normal to the (χ, ξ) plane, either upward (+) or downward (−). Contour lines for positive (red online) and negative (blue online) CDOs are plotted for values of $\Delta n_\lambda(R, \zeta)$ (with $R \equiv (\chi, 0)$) equal to $2^{-k} \times 10^{-4}$ au and $-2^{-k} \times 10^{-4}$ au, respectively, with $k = 0, 1, 2, \ldots, 7$.

CDO is large. In Cu(111) this condition is clearly fulfilled by the $S_3(\bar{M})$ subsurface resonance, as seen in figures 16(d) and (f), which is therefore a good candidate for an explanation of the measurements by Gawronski *et al*. Figure 17 illustrates this correspondence.

4. Towards a spectroscopy of phonon dispersion curves in thin metal films

Besides the ordinary surface waves, ultrathin metal films on stiffer substrates can guide other kinds of sound waves traveling underneath the surface or even along the interface with the substrate. Like the largely exploited surface acoustic waves, their subsurface companions could have a future in electro- and opto-acoustic devices, thus widely extending their applications spectrum. However, these vibrational modes, long since known in seismology as Sezawa waves [72], could so far be investigated in thin films only in the long-wave limit by means of Brillouin spectroscopy [73–75], whereas their dispersion remained so far elusive to current surface probes. A recent HAS study of the phonon dispersion curves in Pb(111) thin films of different thicknesses [76] seems to solve the problem.

Figure 18 shows an interesting example of dispersion curves of five monolayers (ML) of Pb(111) on a Cu(111) substrate as obtained with HAS by Braun *et al* [76]. Two sets of data are reported for un-annealed (○) and annealed (●) samples. Both sets consist of portions of at least eight different dispersion curves in the $\bar{\Gamma}\bar{K}$ direction of the expected ten dispersion curves with sagittal polarization. Braun *et al* analyzed the data by means of a simple Born–von Kàrmàn force constant model in order to qualitatively associate the dispersion curves to the predicted phonon branches. The effects of the comparatively large surface inward relaxation in the 5 ML Pb(111)/Cu(111) system [77] and of the stiffer interlayer force constant have been considered. The ten calculated sagittal phonon frequencies at the zone center (L_{1-5} and SV_{1-5}), corresponding to standing waves also known as *organ-pipe modes* [78], are shown in figure 18: except for SV_3 and L_1 (probably superimposed to SV_1), they can all be associated with measured branches for the un-annealed sample. The highest mode (SV_5) is shown to correspond to the SV2 resonance of the semi-infinite metal (e.g. figure 14), whereas SV_4 is, surprisingly, a mode localized on the bottom layer at the interface.

An interesting aspect of these measurements, which tells about the rich information obtained with HAS, is the effect of annealing on phonon frequencies. The more compact adjustment of the film to the substrate geometry expected from annealing yields a stiffening of the $SV_{4,5}$ upper doublet, pushing the SV_5 mode above the maximum phonon frequency of bulk Pb, and a general softening of the L modes, especially of L_5. First-principles calculations by Yndurain and Ligato [79][7] of the highest SV_5 frequency in well-equilibrated free-standing Pb(111) films indeed predict this mode to occur slightly above the maximum bulk frequency.

[7] In this work the SV_5 mode at $\bar{\Gamma}$ is called longitudinal, consistent with its wave-like extension normal to the film plane.

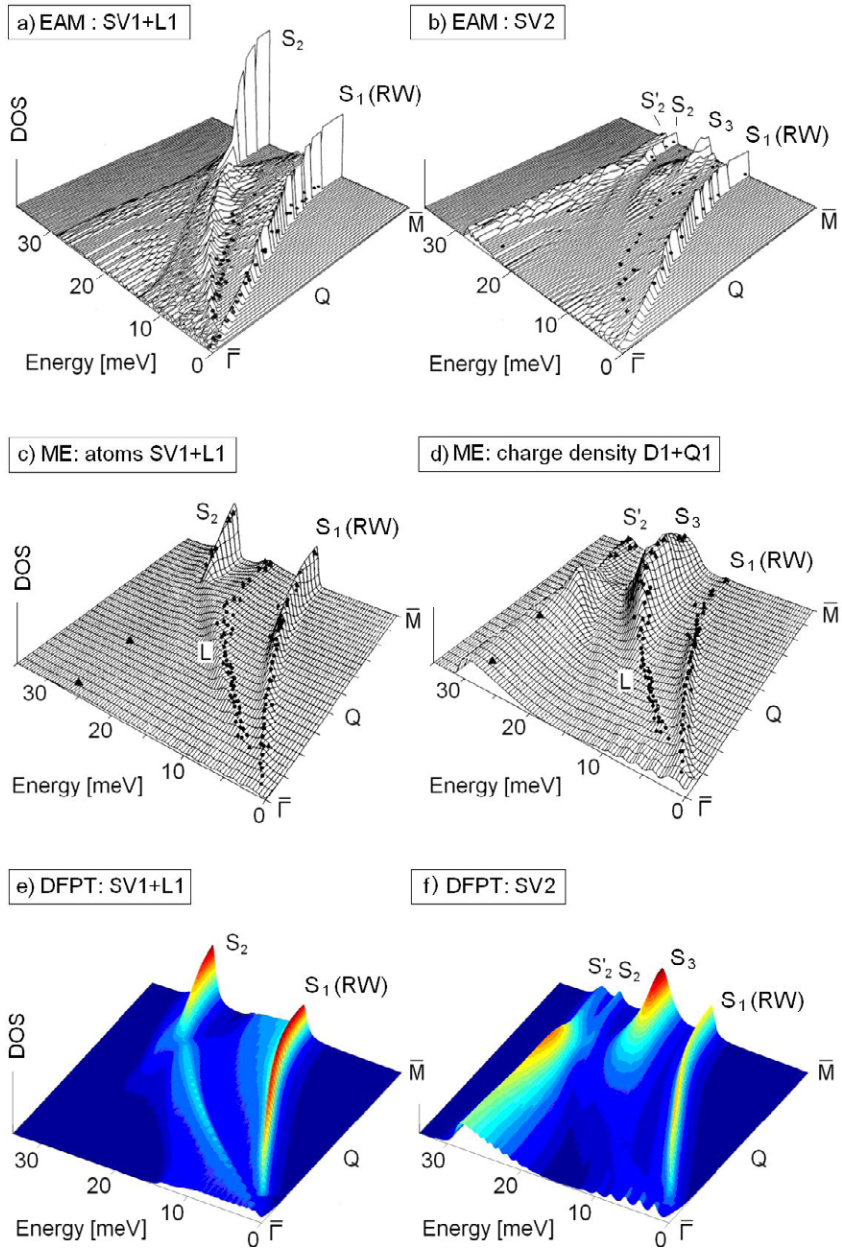

Figure 16. The first-layer phonon sagittal DOS (SV1 + L1) calculated in the $\bar{\Gamma}\bar{M}$ direction of Cu(111) with the embedded-atom method (EAM) [20] (a) and the multiple expansion (ME) method [25] (c) compare very well with the corresponding first-principles DOS calculated with DFPT [39] (e). A similar good agreement is found between the second-layer DOSs for SV polarization between EAM (b) and DFPT (f) calculations, thus showing the ability of EAM to predict the surface optical branches and their hybridization schemes. On the other hand, the phonon DOS projected onto the dipolar (D1) and quadrupolar (Q1) components of the first-layer charge density oscillation (CDO) obtained with the ME method [25] (d) compares very well with both EAM and DFPT DOSs for SV modes in the second layer ((b) and (f)). This shows that, in agreement with the DFPT results of figure 14, the surface CDO reflects the SV motion of the underlying second-layer atoms, thus explaining the sensitivity of HAS to subsurface resonances.

An extensive DFPT calculation, to appear soon [80] of the phonon dispersion curves and associated surface CDOs for Pb(111) films of different thicknesses is indeed providing an accurate interpretation of these recent results, thus confirming that the gentlest of all surface probes, helium atom beams, can actually measure the dispersion of most subsurface phonons. He atoms, though flying-by a few ångströms above the surface, perceive the motion of the underground atoms via the CDOs produced at the surface. According to these calculations [80] this mechanism appears to work best for ultrathin metal films with a highly responsive density of conduction electrons, such as lead.

Another interesting example where a few subsurface modes could be measured with HAS besides the RW dispersion is that of a 6 ML film of fcc-Fe(001) on a Cu(001) substrate [81][8]. The data and the calculated dispersion curves

[8] In this paper details are given about the force constant fit of the dispersion curves shown in figure 19, but not the figure itself, due to lack of space.

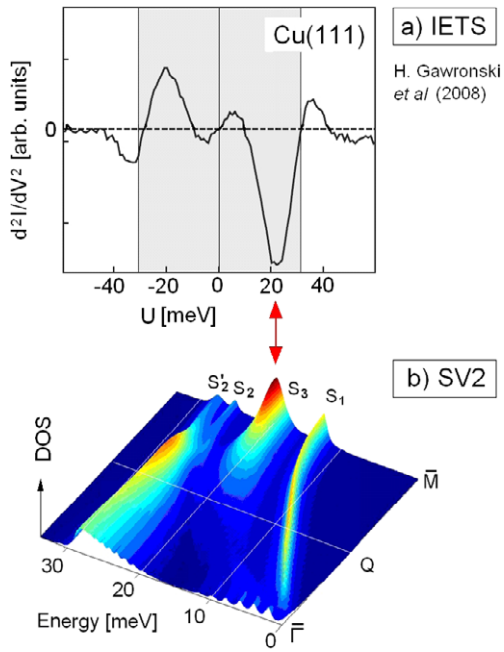

Figure 17. The inelastic electron tunneling spectrum (IETS) collected with an STM tip from the Cu(111) surface [71] shows a large feature at about 21 meV on both the loss and gain sides which can be associated with the large second-layer S_3 resonance.

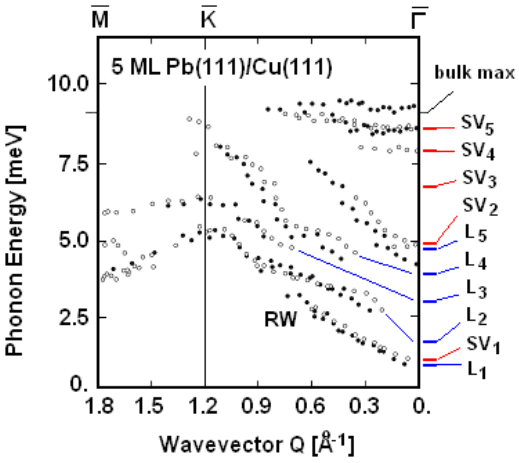

Figure 18. Dispersion curves of a Pb(111) 5 ML film deposited on Cu(111) measured with HAS for an un-annealed (○) and an annealed (●) sample. Symbols L_j and SV_j indicate the zone-center phonon energies for L and SV polarizations, respectively, as derived from a Born–von Kàrmàn force constant fit (adapted from [76]). For a 5 ML film the subscript $j = 1$–5 labels the five standing waves (organ-pipe modes) for each polarization in ascending order.

shown in figure 19 complement the information reported in [81] (see footnote 8) about the effect of magnetization on the RW frequency, and refer to the film below the Curie temperature, with a distorted fcc structure and a sequence (↑↑↓↓↑↑) of ferromagnetic layers. As explained in [81] (see footnote 8) the interatomic force constants include the contributions of exchange interaction. The set of experimental data above the RW is too limited for any further discussion. They should serve, however, as a stimulus for further HAS

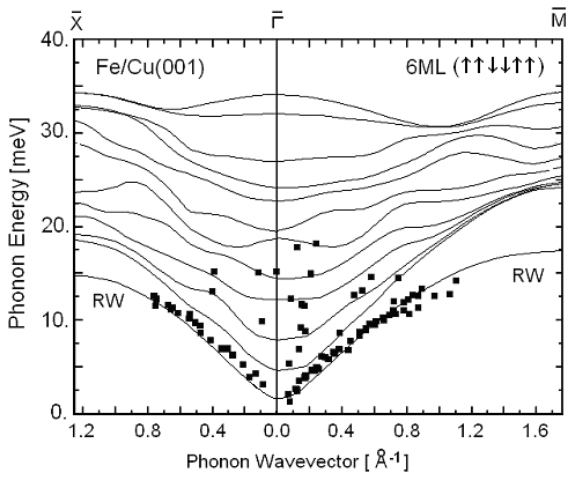

Figure 19. Experimental HAS data points for a 6 ML–fcc-Fe(001)/Cu(001) in the magnetic phase and the dispersion curves calculated with a force constant model including the exchange contributions [81] (see footnote 8).

investigations of the phonon dispersion curves of ultrathin magnetic metal films. More complete sets of dispersion curves would allow us to extract information about the interlayer force constants and to extract the interlayer exchange contributions.

The vibrational spectra of ultrathin bcc-Fe(110) films grown on a W(110) substrate have been recently studied [82, 83] with the novel technique of nuclear inelastic scattering (NIS) of synchrotron radiation [84], which allows for a selective analysis of the phonon DOS projected on single layers. A peculiarity of this spectroscopy is the dominant response from the longitudinal components of the atomic displacements. The analysis of these experimental results, supported by first-principles calculations based on the slab-filling technique with the Hellmann–Feynman forces calculated in the direct space (*direct method*) [85, 86], show important differences between the DOS projected onto the surface and the one projected onto the second layer. This difference is well accounted for by theory [86, 83] and is qualitatively similar to the one expected between the integrated L1 and L2 DOSs of Al(001) and Cu(111) (in the $\bar{\Gamma}\bar{K}$ direction) (figures 3 and 13, respectively). The study of magnetic metal surfaces will hopefully profit also from the recent progress in high-resolution spin-echo ^{3}He scattering spectroscopy [87, 88]. This technique suggests the intriguing question of inelastic HAS from surface (and subsurface) magnetic excitations via induced spin density oscillations.

5. New trends

The recent progress in experimental techniques, like HAS and its evolution into ^{3}He spin-echo spectroscopy, STM-IETS and NIS with synchrotron radiation, will likely extend the surface phonon spectroscopy to a variety of surface processes where surface phonons are involved, and systems, including ultrathin metal films. All these developments call for a further refinement of first-principles theoretical methods. A quick overview of the work done in the field of surface phonons in

metals during the last decade indicates a few relevant trends which have emerged in this field.

One of these concerns *simple metals*, specifically alkali and alkali-earth metals. Although the surface dynamics of sodium surfaces has been tackled with *ab initio* methods already in the early 1980s (for a review see [36]), greater theoretical interest arose in the late 1990s around Be(0001) surface dynamics [89–91] after a series of EELS measurements [92–94]. This eventually stimulated further DFPT studies on the more exotic Be($10\bar{1}0$) surface [95] and, more recently, on Mg(0001) [96]. At about the same time HAS studies of the surface phonon dispersion curves have been carried out for Na(110) [78], Ba(0001) [97], and the low-index surfaces of K [98, 99], Rb [100] and Cs [99, 101] all in the form of ultrathin films on various substrates. Moreover an EELS study is available for 1 and 2 ML of Li(110) on Mo(110) [102] in connection with the Kohn anomaly of the substrate. This new vogue of measurements is accompanied by a few phonon calculations for simple metal surfaces based on the EA method, which proves to be quite efficient for free-electron metals [103–105].

Another important direction actively pursued in this decade is the dynamics of *vicinal surfaces*. The interest in vicinal surfaces dates back to the pioneering EELS studies by Ibach and Bruchmann on Pt(332) and (775) [106] and later studies with HAS on Ni(977) [107–109], Cu(211) and (511) [110]. The large surface unit cell characterizing a vicinal surface and the corresponding extension of the surface perturbation make the use of DFPT computationally heavy. Thus most studies of surface phonons at vicinal surfaces of Al, Cu, Ag, Au, Pd and Ni have been carried out originally by directly using the EA method [111–114, 21, 115–118] and later with a Green's function treatment applied to the EA method [119, 120]. Also a new semi-empirical approach, the tight-binding second-moment (TBSM) total energy method devised by Raouafi *et al* [121], proves effective in the study of phonon dynamics at the vicinal surfaces of copper.

Another interesting class of surface systems drawing the interest of theoreticians are *clusters grown on metals*. As was recently shown by using tight-binding interatomic potentials, the cluster structure and relaxations as well as the vibrational modes are strongly modified by cluster metal surface interactions [122]. The importance of nanoclusters in many relevant dynamical and chemical processes at surfaces, including *heterogeneous catalysis*, and the role of surface phonons have been conjectured since the early days of surface dynamics, though only the advent of *ab initio* approaches to surface dynamics like DFPT can give those conjectures a microscopic basis. On the front of interesting surface systems for heterogeneous catalysis new high-resolution EELS measurements on the hydrogen-covered Pt(111) surface [123, 124] have stimulated further first-principles calculations of the surface dynamics of this important system [125] as well as of the unreconstructed and (2×1) reconstructed clean Pt(110) surface [126].

Last but not least among the new directions is the investigation of *non-adiabatic effects*. A state-of-the-art survey on the experimental and theoretical studies of the surface electron–phonon interaction is found in the excellent review by Kröger [127]. The limited performance of DFPT [128] in explaining the deep Kohn anomaly found in W(110):H(1×1) [129], and also in Mo(111):H(1×1) [130, 131] and $Mo_{1-x}Re_x$(110):H(1×1) [132], may be attributed to the intrinsic non-adiabatic nature of the anomaly, which originates from the hybridization (avoided crossing) of the surface phonon branches with the quasi-1D electron–hole excitation branch [50]. The close correspondence of the anomaly wavevector with a $2k_F$ nesting of the Fermi surface [133, 134] and the small gap determined by the deep anomaly minimum may also be attributed to the formation of a charge density wave (CDW), whose spectrum consists of a phason and an ampliton branch, besides that of the ordinary acoustic phonon. This mechanism, suggested long ago by Giuliani and Tosatti [135], accounts quite well for the anomalous dispersion as observed by HAS [50].

The subsequent discovery by HAS of a surface phase transition in the above systems triggered by the addition of hydrogen and its relationship with the Kohn anomaly [136] offers another aspect of non-adiabatic electron–phonon coupling. A novel approach called complex Dyson non-adiabatic dynamics (CNDA) has been recently formulated and applied by Eiguren *et al* [137–139] to the clean W(110) surface as well as to W(110):H(1×1) and MgB_2, providing a clear quantitative picture of the mixing between surface phonons and electron–hole excitations.

These are just a few of the most significant trends in the dynamical theory of metal surfaces. The role played by surface phonons in a growing variety of dynamical phenomena at metal surfaces of both fundamental and applicative interest can be better appreciated in some recent series of papers appearing in the present journal [140, 141].

Acknowledgment

One of us (GB) gratefully acknowledges the support of IKERBASQUE (Project ABSIDES).

References

[1] Doak R B, Harten U and Toennies J P 1983 *Phys. Rev. Lett.* **51** 578
[2] Harten U, Toennies J P and Wöll Ch 1985 *Faraday Discuss. Chem. Soc.* **80** 137
[3] Feuerbacher B and Willis R F 1981 *Phys. Rev. Lett.* **47** 526
[4] Benedek G and Toennies J P 1994 *Surface Science: The First Thirty Years* ed C B Duke (Amsterdam: North-Holland)
Benedek G and Toennies J P 1994 *Surf. Sci.* **299/300** 587
[5] Benedek G and Toennies J P 2010 *Surface Phonons Spectroscopy by Helium Atom Scattering* (Heidelberg: Springer) to be published
[6] Ibach H and Mills D L 1982 *Electron Energy Loss Spectroscopy and Surface Vibrations* (New York: Academic)
[7] Mohamed M H, Kesmodel L L, Hall B M and Mills D L 1988 *Phys. Rev.* B **37** 2763
[8] Hall B M, Mills D L, Mohamed M H and Kesmodel L L 1988 *Phys. Rev.* B **38** 5856
[9] Mohamed M H and Kesmodel L L 1988 *Phys. Rev.* B **37** 6519
[10] Rocca M 2002 *Surface Phonon Dispersion* (*Landolt-Börstein, New Series III/42.A2/4.5*) (Berlin: Springer)

[11] Bortolani V, Franchini A, Nizzoli F and Santoro G 1984 *Phys. Rev. Lett.* **52** 429
[12] Bortolani V, Santoro G, Harten U and Toennies J P 1984 *Surf. Sci.* **148** 82
[13] Bortolani V, Franchini A and Santoro G 1985 *Electronic, Dynamic and Quantum Structural Properties of Condensed Matter* ed J T Devreese and P E van Camp (New York: Plenum) p 401
[14] Armand G 1983 *Solid State Commun.* **48** 261
[15] Toennies J P 1990 *Superlatt. Microstruct.* **7** 193
[16] Zangwill A 1988 *Physics at Surfaces* (Cambridge: Cambridge University Press)
[17] Ibach H and Lüth H 1996 *Solid-State Physics* 2nd edn (Berlin: Springer)
[18] Daw M S and Baskes M I 1984 *Phys. Rev.* B **29** 6443
[19] Nelson J S, Sowa E C and Daw M S 1988 *Phys. Rev. Lett.* **61** 1977
[20] Nelson J S, Daw M S and Sowa E C 1989 *Phys. Rev.* B **40** 1465
[21] Chulkov E V and Sklyadneva I Y 1995 *Surf. Sci.* **331–333** 1414
[22] Eiguren A, Hellsing B, Chulkov E V and Echenique P M 2003 *Phys. Rev.* B **67** 235423
[23] Borisova S D, Rusina G G, Eremeev S V, Benedek G, Echenique P M, Yu Sklyadneva I and Chulkov E V 2006 *Phys. Rev.* B **74** 165412
[24] Jayanthi C S, Bilz H, Kress W and Benedek G 1987 *Phys. Rev. Lett.* **59** 795
[25] Kaden C, Ruggerone P, Toennies J P, Zhang G and Benedek G 1992 *Phys. Rev.* B **46** 13509 In this work the phenomenological model derived from the multiple expansion concept is termed pseudocharge (PC) method
[26] Benedek G, Ellis J, Luo N S, Reichmuth A, Ruggerone P and Toennies J P 1993 *Phys. Rev.* B **48** 4917
[27] Beatrice C and Calandra C 1983 *Phys. Rev.* B **28** 6130
[28] Gaspar J A and Eguiluz A G 1989 *Phys. Rev.* B **40** 11976
[29] Eguiluz A G, Gaspar J A, Gester M, Lock A and Toennies J P 1990 *Superlatt. Microstruct.* **7** 223
[30] Gaspar J A, Eguiluz A G, Gester M, Lock A and Toennies J P 1991 *Phys. Rev. Lett.* **66** 337
[31] Franchini A, Bortolani V, Santoro G, Celli V, Eguiluz A G, Gaspar J A, Gester M, Lock A and Toennies J P 1993 *Phys. Rev.* B **47** 4691
[32] Bohnen K P and Ho K M 1988 *Surf. Sci.* **207** 105
[33] Ho K M and Bohnen K P 1990 *J. Electron Spectrosc. Relat. Phenom.* **54/55** 229
[34] Chen Y, Tong S Y, Bohnen K P, Rodach T and Ho K M 1993 *Phys. Rev. Lett.* **70** 603
[35] Tong S Y, Chen Y, Bohnen K P, Rodach T and Ho K M 1994 *Surf. Rev. Lett.* **1** 97
[36] Heid R and Bohnen K-P 2003 *Phys. Rep.* **387** 151
[37] Baroni S *et al* 2001 *Rev. Mod. Phys.* **73** 515
[38] Chis V, Hellsing B, Benedek G, Bernasconi M and Toennies J P 2007 *J. Phys.: Condens. Matter* **19** 305011
[39] Chis V, Hellsing B, Benedek G, Bernasconi M, Chulkov E V and Toennies J P 2008 *Phys. Rev. Lett.* **101** 206102
[40] Hofmann Ph, Sklyadneva I Y, Rienks E D L and Chulkov E V 2009 to be published
[41] da Silva J L F 2005 *Phys. Rev.* B **71** 195416
[42] Berndt W, Weick D, Stampfl C, Brashaw A M and Scheffler M 1995 *Surf. Sci.* **330** 182
[43] Petersen H, Mikkelsen A, Nielsen M M and Adams D L 1999 *Phys. Rev.* B **60** 5963
[44] Perdew J P, Burke K and Ernzerhof M 1996 *Phys. Rev. Lett.* **77** 3865
[45] Bortolani V, Franchini A, Nizzoli F, Santoro G, Benedek G and Celli V 1983 *Surf. Sci.* **128** 249
[46] Lucas A A 1968 *J. Chem. Phys.* **48** 3156
[47] Benedek G 1996 Lucas modes *Phys. Mag.* **18** 205–14
[48] Wallis R F 1957 *Phys. Rev.* **105** 540
Wallis R F 1959 *Phys. Rev.* **116** 302
[49] Sklyadneva I Y, Chulkov E V and Echenique P M 2007 *J. Phys.: Condens. Matter* **20** 165203
[50] Benedek G, Pardo M and Toennies J P 2007 *Highlights on Spectroscopies of Semiconductors and Nanostructures* (*Conf. Proc.* vol 94) ed G Guizzetti, A C Andreani, F Marabelli and M Patrini (Bologna: SIF) pp 151–67
[51] Yu H and Hermanson J C 1989 *Phys. Rev.* B **40** 11851
Yu H and Hermanson J C 1990 *Phys. Rev.* B **41** 5991
[52] Diaconescu B, Pohl K, Vattuone L, Savio L, Hofmann P, Silkin V M, Pitarke J M, Chulkov E V, Echenique P M, Farìas D and Rocca M 2007 *Nature* **448** 57
[53] Silkin V M, Pitarke J M, Chulkov E V, Diaconescu B, Pohl K, Vattuone L, Savio L, Hofmann Ph, Farias D, Rocca M and Echenique P M 2008 *Phys. Status Solidi* a **205** 1307
[54] Silkin V M, García-Lekue A, Pitarke J M, Chulkov E V, Zaremba E and Echenique P M 2004 *Europhys. Lett.* **66** 260
[55] Silkin V M, Pitarke J M, Chulkov E V and Echenique P M 2005 *Phys. Rev.* B **72** 115435
[56] dal Corso A 2001 *Phys. Rev.* B **64** 235118
[57] Chae K H, Lu H C and Gustafsson T 1996 *Phys. Rev.* B **54** 14082
[58] Lindgren S-Å, Walldén L, Rundgren J and Westrin P 1984 *Phys. Rev.* B **29** 576
[59] Bohnen K-P and Ho K M 1993 *Surf. Sci. Rep.* **19** 99
[60] Hennig D, Ganduglia-Pirovano M V and Scheffler M 1996 *Phys. Rev.* B **53** 10344
[61] Da Silva J L F, Stampfl C and Scheffler M 2006 *Surf. Sci.* **600** 703
[62] Foiles S M, Baskes M I and Daw M S 1986 *Phys. Rev.* B **33** 7983
[63] Ditlevsen P D and Nørskov J K 1990 *J. Electron Spectrosc. Relat. Phenom.* **54/55** 237
[64] Ditlevsen P D and Nørskov J K 1991 *Surf. Sci.* **254** 261
[65] Chen Y, Tong S Y, Bohnen K P, Rodach T and Ho K M 1993 *Phys. Rev. Lett.* **70** 603
[66] Tong S Y, Chen Y, Bohnen K P, Rodach T and Ho K M 1994 *Surf. Rev. Lett.* **1** 97
[67] Bortolani V and Levi A C 1986 *Riv. Nuovo Cimento* **9** 1
[68] Esbjerg N and Norskov J K 1980 *Phys. Rev. Lett.* **45** 807
[69] Cole M W and Toigo F 1985 *Phys. Rev.* B **31** 727
[70] Lorente N and Persson M 2000 *Phys. Rev. Lett.* **85** 2997
[71] Gawronski H, Mehlhorn M and Morgenstern K 2008 *Science* **319** 930
[72] Sezawa K 1927 Dispersion of elastic waves propagating on the surface of stratified bodies and on curved surfaces *Bull. Earthq. Res. Inst. Univ. Tokyo* **3** 1
[73] Bortolani V, Marvin A M, Nizzoli F and Santoro G 1983 *J. Phys. C: Solid State Phys.* **16** 1751
[74] Stegeman G I and Nizzoli F 1984 *Surface Excitations* ed V M Agranovich and R Loudon (Amsterdam: Elsevier Science) p 195
[75] Zhang X, Bandhu R S, Sooryakumar R and Jonker B T 2003 *Phys. Rev.* **67** 075407
[76] Braun J, Ruggerone P, Zhang G, Toennies J P and Benedek G 2009 *Phys. Rev.* B **79** 205423
[77] Jia Y, Wu B, Weitering H H and Zhang Z 2006 *Phys. Rev.* B **74** 35433
[78] Benedek G, Ellis J, Reichmuth A, Ruggerone P, Schief H and Toennies J P 1992 *Phys. Rev. Lett.* **69** 2951
[79] Yndurain F and Jigato M P 2008 *Phys. Rev. Lett.* **100** 205501
[80] Sklyadneva I Y, Chulkov E V, Echenique P M, Heid R, Bohnen K-P, Benedek G and Toennies J P 2009 to be published
[81] Benedek G, Hulpke E and Steinhögl W 2001 *Phys. Rev. Lett.* **87** 027201
[82] Ślęzak T *et al* 2007 *Phys. Rev. Lett.* **99** 066103

[83] Stankov S *et al* 2007 *Phys. Rev. Lett.* **99** 185501
[84] Röhlsberger R 2004 *Nuclear Condensed Matter Physics with Synchrotron Radiation* (*Springer Tracts in Modern Physics* vol 208) (Berlin: Springer)
[85] Parlinski K 2006 *Phys. Rev.* B **74** 184309
[86] Łażewski J, Korecki J and Parlinski K 2007 *Phys. Rev.* B **75** 054303
[87] Jardine A P, Dworski S, Fouquet P, Alexandrowicz G, Riley D J, Lee G Y H, Ellis J and Allison W 2004 *Science* **304** 1790
[88] Alexandrowicz G and Jardine A P 2007 *J. Phys.: Condens. Matter* **19** 305001
[89] Kwasniok F 1995 *Surf. Sci.* **329** 90
[90] Pohl K, Cho J H, Terakura K, Scheffler M and Plummer E W 1998 *Phys. Rev. Lett.* **80** 2853
[91] Lazzeri M and de Gironcoli S 1998 *Phys. Rev. Lett.* **81** 2096
Lazzeri M and de Gironcoli S 1998 *Surf. Sci.* **402–404** 715
[92] Hannon J B and Plummer E W 1993 *J. Electron Spectrosc. Relat. Phenom.* **64/65** 683
[93] Plummer E W and Hannon J B 1994 *Prog. Surf. Sci.* **46** 149
[94] Hannon J B, Mele E J and Plummer E W 1996 *Phys. Rev.* B **53** 2090
[95] Lazzeri M and de Gironcoli S 2000 *Surf. Sci.* **454** 442
[96] Leonardo A, Yu Sklyadneva I, Silkin V M, Echenique P M and Chulkov E V 2007 *Phys. Rev.* B **76** 035404
[97] Bartholmei S, Fouquet P and Witte G 2001 *Surf. Sci.* **474** 222
[98] Fuhrmann D, Hulpke E and Steinhögl W 1998 *Phys. Rev.* B **57** 4798
[99] Hulpke E, Lower J and Reichmuth A 1996 *Phys. Rev.* B **53** 13901
[100] Flach B, Hulpke E and Steinhögl W 1998 *Surf. Sci.* **412** 12
[101] Senet P, Toennies J P and Witte G 1999 *Chem. Phys. Lett.* **229** 389
[102] Kröger J, Bruchmann D, Lehwald S and Ibach H 2000 *Surf. Sci.* **449** 227
[103] Sklyadneva I Y, Chulkov E V and Bertsch A V 1996 *Surf. Sci.* **352** 25
[104] Riffe D M and Wertheim G K 2000 *Phys. Rev.* B **61** 2302
[105] Rusina G G, Eremeev S V, Echenique P M, Benedek G, Borisova S D and Chulkov E V 2008 *J. Phys.: Condens. Matter* **20** 224007
[106] Ibach H and Bruchmann D 1978 *Phys. Rev. Lett.* **41** 958
[107] Niu L, Gaspar D J and Sibener S J 1995 *Science* **268** 847
[108] Niu L, Koleske D D, Gaspar D J and Sibener S J 1995 *J. Chem. Phys.* **102** 9077
[109] Gaspar D J, Hanbicki A T and Sibener S J 1998 *J. Chem. Phys.* **109** 6947
[110] Witte G, Braun J, Lock A and Toennies J P 1995 *Phys. Rev.* B **52** 2165
[111] Bertsch A V, Eremeev S V, Lipnitskii A G, Yu Sklyadneva I and Chulkov A V 1994 *Fiz. Tverd. Tela* **36** 2935
[112] Tian Z-J and Black J E 1994 *Surf. Sci.* **303** 395
[113] Kara A, Jayanthi C S, Wu S Y and Ercolessi F 1994 *Phys. Rev. Lett.* **72** 2223
[114] Kara A, Jayanthi C S, Wu S Y and Ercolessi F 1995 *Phys. Rev.* B **51** 17046
[115] Rusina G G, Berch A V, Sklyadneva I Y, Eremeev S V, Lipnitskii A G and Chulkov E V 1996 *Fiz. Tverd. Tela.* **38** 141
[116] Kara A, Durukanoglu S and Rahman T S 1996 *Phys. Rev.* B **53** 15489
[117] Durukanoglu S, Kara A and Rahman T S 1997 *Phys. Rev.* B **55** 13894
[118] Yu Sklyadneva I, Rusina G G and Chulkov E V 1998 *Surf. Sci.* **416** 17
[119] Kara A, Staikov P, Rahman T S, Radnik J, Biagi R and Ernst H-J 2000 *Phys. Rev.* B **61** 5714
[120] Kara A and Rahman T S 2005 *Surf. Sci. Rep.* **56** 159
[121] Raouafi F, Barreteau C, Desjonquères M C and Spanjaard D 2002 *Surf. Sci.* **507** 748
[122] Borisova S D, Eremeev S V, Rusina G G, Stepanyuk V S, Bruno P and Chulkov E V 2008 *Phys. Rev.* B **78** 075428
[123] Badescu S C, Salo P, Ala-Nissila T, Ying S C, Jacobi K, Wang Y, Bedürftig K and Ertl G 2002 *Phys. Rev. Lett.* **88** 136101
[124] Badescu S C, Jacobi K, Wang Y, Bedürftig K, Ertl G, Salo P, Ala-Nissila T and Ying S C 2003 *Phys. Rev.* B **68** 205401
[125] Hong S, Rahman T S, Heid R and Bohnen K P 2005 *Surf. Sci.* **587** 41
[126] Hong S, Rahman T S, Heid R and Bohnen K P 2005 *Phys. Rev.* B **72** 205424
[127] Kröger J 2006 Electron–phonon coupling at metal surfaces *Rep. Prog. Phys.* **69** 899–969
[128] Bungaro C, de Gironcoli S and Baroni S 1996 *Phys. Rev. Lett.* **77** 2491
[129] Hulpke E and Lüdecke J 1992 *Phys. Rev. Lett.* **68** 2846
[130] Hulpke E and Lüdecke J 1993 *Surf. Sci.* **287/288** 837
[131] Hulpke E and Lüdecke J 1993 *J. Electron Spectrosc. Relat. Phenom.* **64/65** 641
[132] Okada M, Flach B, Hulpke E, Steinhögel W and Plummer E W 2002 *Surf. Sci.* **498** L78
[133] Kohler B, Ruggerone P and Scheffler M 1996 *Surf. Sci.* **368** 213
[134] Kohler B, Ruggerone P, Scheffler M and Tosatti E 1996 *Z. Phys. Chem.* **197** 193
[135] Giuliani G and Tosatti E 1978 *Nuovo Cimento* B **47** 135
Giuliani G and Tosatti E 1979 *Quasi-One Dimensional Conductors* ed S Baricic, A Bjelis, J R Cooper and B Leontic (Berlin: Springer) p 191
See also Tosatti E 1995 *Electronic Surface and Interface States on Metallic Systems* ed E Bertel and M Donath (Singapore: World Scientific) p 67
[136] Yamada Y, Rieder K-H and Theis W 2007 *Phys. Rev. Lett.* **99** 196105
[137] Eiguren A and Ambrosch-Draxl C 2008 *Phys. Rev. Lett.* **101** 036402
[138] Eiguren A and Ambrosch-Draxl C 2008 *Phys. Rev.* B **78** 045124
[139] Eiguren A, Ambrosch-Draxl C and Echenique P M 2009 *Phys. Rev.* B **79** 5103
[140] Franchini A and Santoro G (ed) 2007 *Proc. 12th Workshop on Surface Dynamics*; *J. Phys.: Condens. Matter* **19** 300301
[141] Benedek G and Vattuone L (ed) 2008 *VAS 12: Proc 12th Int. Conf. on Vibrations at Surfaces*; *J. Phys.: Condens. Matter* **20** 220301